Journal of Manufacturing Science and Mechanical Engineering
Print ISSN: 2959-9881
Online ISSN: 2959-989X
DOI: https://doi.org/10.61784/msme3022

A BIOLOGICALLY INSPIRED MODEL FOR THE DEVELOPMENT OF HEAD-DIRECTION CELLS IN THE RAT BRAIN USING VISUAL INPUT

YiShen Liao*, HuaYang Li, Yun Zhang, AiHua Zhao, HaoDong Qin, Lang Chen, QingShan Chen
Modern Industry School of Virtual Reality, Jiangxi University of Finance and Economics, Nanchang 330013, Jiangxi, China.
**Corresponding Author: YiShen Liao*

Abstract: Head direction cells (HDCs), located in the entorhinal cortex and postsubiculum of the rat brain, exhibit specific firing patterns corresponding to head direction, primarily driven by visual input. This study proposes a biologically inspired computational model for HDCs development using visual information as the primary input. The model employs a one-dimensional annular cell structure, where neural activity is driven by optical flow calculated via the Lucas-Kanade algorithm and corrected through visual template matching and the PI controller. This closed-loop mechanism simulates the maturation process of HDCs, enabling the neural activity package to accurately track the real head-direction angle. Experimental results show that the model not only demonstrate the developmental process of HDCs, but also achieves precise head-direction estimation with significantly reduced cumulative errors compared to traditional gyroscope-based methods, offering a low-hardware-requirement solution. The model not only replicates the development of HDCs but also lays a foundation for bio-inspired navigation systems, with potential applications in robotics and cognitive modeling.
Keywords: Head-direction cells; Visual input; Entorhinal cortex; Developmental process; Bio-inspired navigation

1 INTRODUCTION

Spatial navigation is a fundamental cognitive ability, enabling animals to orient themselves and move effectively within their environments [1]. In the rat brain, this process is mediated by a network of specialized neurons, including place cells, grid cells, and head-direction cells, located in the hippocampus and entorhinal cortex [2-4]. These neurons integrate sensory and self-motion information to construct a cognitive map that represents the animal's position and orientation relative to its surroundings [5-6]. A central question in neuroscience is whether spatial cells possess innate functional properties at birth or whether their specific firing patterns emerge through postnatal development and environmental interaction. Physiological studies provide critical insights into this question. For instance, Wills et al. demonstrated that HDCs in the rat brain exhibit mature electrophysiological characteristics at birth, in contrast to place and grid cells, which develop their spatial specificity later [7]. This suggests that directional information forms the foundation of spatial cognition in rats.

Head-direction cells, first discovered by Taube et al. in the rat postsubiculum and later identified in the entorhinal cortex, fire maximally when the rat's head is oriented in a specific direction, with their firing rate decreasing as the head deviates from this preferred direction, approximated by a Gaussian function [8-9]. These cells receive inputs from multiple sensory modalities, with vestibular and visual systems being particularly critical [10]. The vestibular system, which detects head rotation through sensory cells in the inner ear, provides angular velocity information that is transmitted to HDCs via neural pathways [11-12]. However, visual input dominates environmental perception, comprising roughly 70% of the sensory data processed by mammals [13-14]. The continuous change in retinal images, known as visual flow, enables animals to estimate both the direction and speed of their movements, making it a vital component of spatial navigation [15-16]. This interplay between vestibular and visual inputs allows HDCs to maintain accurate directional representations, even in dynamic or unfamiliar environments [17].

The development of HDCs is critical for biological navigation but poorly understood, limiting bioinspired improvements in robotic navigation systems that face errors with traditional sensors like gyroscopes [18]. To address this, we propose a computational model of HDCs development in the rat brain, with the following innovations:

(1) Annular HDCs model with visual input. Proposing a model that uses only visual information as input to construct an annular cell model, simulating the firing activity of HDCs, achieving synchronization between neural activity and the actual head-direction angle.

(2) Closed-loop correction mechanism for simulating cell maturation. The model incorporates visual closed-loop detection and reference point update algorithms, enabling convergence to a state consistent with the actual angle through multiple rotation experiments, thus achieving dynamic simulation of HDCs development from initial immaturity to gradual maturity.

(3) Low-hardware-requirement head direction estimation. Unlike traditional methods that rely on both gyroscope and camera, this model employs visual template matching and PI controller to dynamically adjust vestibular gain, significantly reducing angular cumulative errors.

The subsequent structure of this article is outlined below. Section 2 revisit pertinent studies and discuss the shortcomings

of previous research endeavors. Section 3 delves into the various details of model construction. Experimental findings are exhibited in Section 4, followed by the conclusion in Section 5.

2 RELATED WORKS

The modeling of HDCs have garnered significant attention in neuroscience and robotics due to their critical role in spatial navigation and their potential to inform bio-inspired algorithms. This section reviews prior work from the perspectives of sensory integration mechanisms, computational architectures for HDCs simulation, and their applications in robotics.

2.1 Sensory Integration in Head-Direction Systems

Sensory integration in head-direction systems refers to the brain's ability to combine multiple sensory inputs to maintain an accurate sense of spatial orientation and direction. HDCs integrate diverse sensory cues, including visual landmarks, vestibular signals from head movements, and proprioceptive feedback from body position [19]. For instance, visual cues provide stable environmental references, while vestibular inputs track angular head velocity, and proprioceptive signals help update orientation based on self-motion [20]. The integration process involves complex neural computations, primarily in structures like the hippocampus and entorhinal cortex, where multisensory information is synthesized to ensure robust and accurate directional representation, even in the absence of external cues [21]. This dynamic interplay allows animals to navigate effectively, adapting to environmental changes or sensory disruptions, and is a critical model for understanding spatial cognition and navigation in mammals.

2.2 Error Correction and Visual Feedback in Robotics

Error correction is a critical challenge in both biological and robotic navigation. In mammals, visual landmarks and optic flow help correct errors in vestibular-based path integration. In 2008, Milford et al. developed a brain-like SLAM system, RatSLAM, using a single camera to map a suburban environment. The system leverages a bionic model with pose cells and visual feedback to construct experience maps, achieving robust error correction and large-scale navigation [22]. In 2021, Zou et al. proposed a brain inspired navigation framework that simulates spatial cells' firing activity and episodic memory self-organization learning, integrating visual feedback to construct cognitive maps, achieving error correction and efficient navigation [23]. In 2024, Zhang et al. proposed a spatial transformation-based continuous attractor network model, simulating place cells and grid cells to integrate information for robot navigation. By leveraging visual cues to correct path integration errors, the model significantly enhances navigation accuracy [24].

2.3 Computational Architectures for HDCs Simulation

Computational architectures for HDCs simulation aim to model the neural mechanisms underlying spatial orientation by replicating the activity of HDCs, which fire selectively based on an agent's head orientation. In 2010, Massoud et al. proposed a hardware-implemented neuromorphic VLSI system that simulates the organization of HDCs, enabling low-power spatial navigation and supporting real-time simulation of spiking neural networks [25]. In 2015, Page et al. investigated the architectural constraints of HDCs networks (such as connection patterns and inhibition) through simulations, revealing factors limiting the accuracy of path integration [26]. In 2022, Vafidis et al. used attractor networks combined with self-supervised learning to simulate how the HDCs learns accurate angular path integration from experience, emphasizing the formation and stability of continuous attractors [27]. In 2024, Westeinde et al. developed a computational model of Drosophila HDCs systems, using phase-shifted sinusoidal representations in PFL neurons to simulate goal-directed steering [28]. In 2025, Sun et al. presented the BIG framework, integrating HDCs models with von Mises firing distributions and geometry cells for robotic navigation, with Monte Carlo simulations showing over 20% improved exploration efficiency through circular statistical analysis of head-direction signals [29].

3 METHODS AND MATERIALS

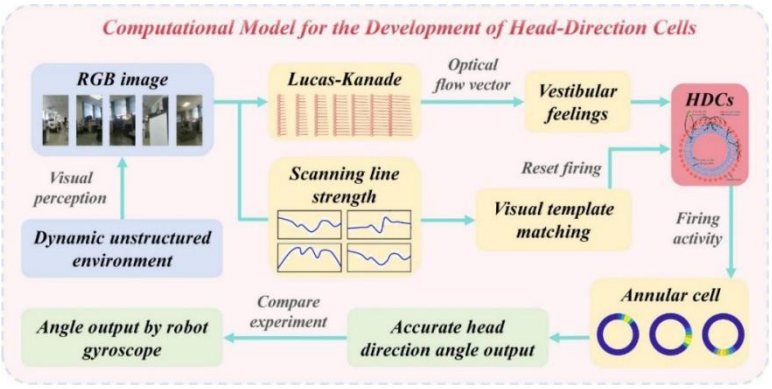

Figure 1 The Overall Operation Mechanism of the Computational Model

In this section, the overall structure of the development model is explained in detail. It is mainly divided into the following aspects. Firstly, The HDCs was modeled as a one-dimensional annular cell model, and the location of the neural activity package on the annular model guided the current head-direction angle. Then, using Lucas-Kanade algorithm to calculate the optical flow vector between two consecutive frames of images, as the forward input signal to stimulate the receptor cells in the vestibular organ. In addition, The scanning line intensity was used as the matching algorithm of view template to correct the vestibular organ output angle integral error and reset the firing activity of the annular model, so that the location of neural activity package on the annular model could gradually follow the change of the real head-direction angle. The overall operation mechanism is shown in Figure 1.

3.1 Acquisition of Visual Drive Singals

Lucas-Kanade algorithm was used to calculate the optical flow field between continuous images as the forward input signal to stimulate the receptor cells in the vestibular organ [30]. Let the original picture be $I(x,y,z,t)$, the time of the previous frame be t, and the time of the next frame be $t+\Delta t$.The position of the pixel point of the previous frame in the next frame is $I(x+\Delta x,y+\Delta y,z+\Delta z,t+\Delta t)$. According to the assumption of constant brightness:

$$I(x,y,z,t)=I(x+\Delta x,y+\Delta y,z+\Delta z,t+\Delta t) \tag{1}$$

For a two-dimensional image, only need to be considered, where I_x,I_y,I_z are the differences of the image in the direction of respectively, which can be written in the following form:

$$I_xV_x+I_yV_y=-I_t \tag{2}$$

According to the spatial consistency hypothesis, it is abbreviated to the following form:

$$\begin{bmatrix} I_{x1} & I_{y1} \\ I_{x2} & I_{y2} \\ \cdots & \\ I_{xn} & I_{yn} \end{bmatrix} \begin{bmatrix} V_x \\ V_y \end{bmatrix} = - \begin{bmatrix} I_{t1} \\ I_{t2} \\ \cdots \\ I_{tn} \end{bmatrix} \tag{3}$$

Then, the optical flow vector can be obtained as follows:

$$\begin{bmatrix} V_x \\ V_y \end{bmatrix} = \begin{bmatrix} \sum {I_{xi}}^2 & \sum I_{xi}I_{yi} \\ \sum I_{yi}I_{xi} & \sum {I_{yi}}^2 \end{bmatrix} \begin{bmatrix} -\sum I_{xi}I_{yi} \\ -\sum I_{yi}I_{xi} \end{bmatrix} \tag{4}$$

In Eq. (4), and represents the magnitude of the optical flow vector on the horizontal and vertical direction. Then, the mathematical expression defining the magnitude of the vestibular drive signal generated by the optical flow vector is shown as follows:

$$v=\beta \sum_{i=0}^{n_g} V_{xi} \tag{5}$$

In Eq. (5), represents the value of the i-th optical flow vector, represents the number of the optical flow vector, represents the information transfer gain of vestibular organs.

3.2 Annular Model and Its Firing Activities

Each HDC corresponds to a maximum firing angle. A one-dimensional gaussian distribution was used to create the excitability weight connection matrix of the HDCs. The variation of the excitability connection toward the cells was as follows:

$$\Delta P_{EH}=\sum_{i=0}^{n_h-1} p_h exp(-\frac{m^2}{x_p}) \tag{6}$$

In Eq. (6), The is the weights of excitatory connection matrix, is the distance between the units on behalf of one dimensional coordinate system coordinates, x_p is the distribution width constant of neural activity, p_h represents the neural activity of the current annular cell model, and is the number of HDCs in the annular model, which represents the range of activity of the nerve wrapped. Each HDC also receives global inhibitory signals from the entire neural network, with the mathematical expression is as follows:

$$\Delta P_{IH}=\sum_{i=0}^{n_h} p_h \psi_m - \varphi \tag{7}$$

In Eq. (7), is the inhibitory connection weights; φ control overall level.In order to ensure that the discharge rate of all head-direction cells is between 0 and 1, the firing rate of all cells is compared with 0, and then standardized. The mathematical expression is as follows:

$$p_{hb}^{t+1}=\frac{max\{p_h^{t+1}+\Delta P_{EH}+\Delta P_{IH}\}}{\sum_{i=0}^{n_h} max\{p_h^{t+1}+\Delta P_{EH}+\Delta P_{IH}\}} \tag{8}$$

In the proposed model, the movement of the neural activity package on the annular model comes from the optical flow, which activates different groups of HDCs and encodes the magnitude of head-direction angle. The firing rate of all cells can be expressed as:

$$p_h^{t+1}=\sum_{m=\delta H_0}^{\delta H_0+1} \alpha_m p_{m+H}^t \tag{9}$$

In Eq. (9), represents the bias of the downward integration of the coordinate system, which is determined by the

direction and magnitude of the optical flow. The mathematical expression is as follows:

$$\delta H_0=\lfloor k_m\vec{e}v\rfloor \tag{10}$$

In Eq. (10), is the angle integral constant. From Eq. (11), it can be seen that the firing rate of HDCs at the next moment is the product of the activity rate of heading toward the cell at the current moment and the parameter α_m. The mathematical expression of is shown in Eq.(11).

$$\alpha_m=\begin{cases}1-\delta H_f, m-\delta H_0=0\\ \delta H_f \quad , m-\delta H_0=0\end{cases} \tag{11}$$

In Eq. (11), represents parameter bias, and its mathematical expression is as follows:

$$\delta H_f=\lfloor k_m\vec{e}v-\delta H_0\rfloor \tag{12}$$

3.3 Construct the Development Model

In fact, the markers of HDCs maturation are that the location of activity package on the annular model strictly followed the change of the head-direction angle. To achieve this goal, the following two conditions need to be met simultaneously. Firstly, the initial position of the activity pack is consistent with the initial head-direction angle. Then, the movement speed of activity package on the annular model is consistent with the change of head-direction angle. As mentioned above, the magnitude of vestibular receptor gain influences the moving speed of the activity package on the annular model. When the moving speed of the active packet is inconsistent with the angular speed of the head-direction change, the accumulated error between the location of the active packet and the head-direction angle will increase gradually over time. The conceptual diagram is shown in Figure 2.

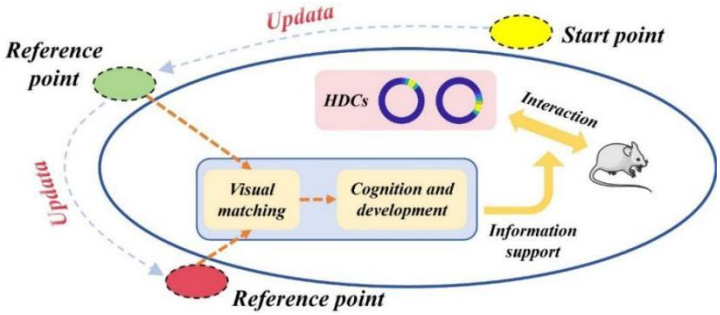

Figure 2 Conceptual Sketch of HDCs Development Model

The algorithm shown in Figure 2 is roughly thought as follows: on the one hand, the current accurate head-direction angle is provided for the model and the firing activity of the annular model is reset by using the way of visual matching. On the other hand, the magnitude of vestibular sensory gain was adjusted at the closed loop point, so that the moving speed of the active pack on the annular model was gradually consistent with the changing speed of the real head-direction angle, and the HDCs development process was realized. The detailed steps of the algorithm are as follows.

Step1: Construction of cognitive points. The robot equipped with camera and gyroscope was used to rotate once in situ at the angular velocity changing all the time. was taken as the sampling period, To construct a cognitive point e with topological relationship at each sampling node. Each cognitive point contained the position when the neural activity was wrapped in the circular model, the head direction angle θ_i, the visual template v_i, and the current moment t_i.

Step2: Establishment of image matching and angle reference node. After rotating from the starting point, the time of reaching the origin again is detected by means of visual matching. In this paper, image scan line intensity matching is used to find the closed-loop image [22]. The principle is as follows: the average absolute intensity difference between the intensity distributions of two image scan lines is calculated, which is called the intensity offset and is represented by $g(c)$.

$$g\left(c,I^j,I^k\right)=\frac{1}{b-|c|}\left(\sum_{i=0}^{n_h}|I^j_{i+\max(c,0)}-I^j_{i-\min(c,0)}|\right) \tag{13}$$

In Eq. (13), and are the scan line intensity distribution of the image being compared, is the distribution offset, and is the width of the image. Setting a comparison threshold c_m. Calculating the intensity offset between the current image and the corresponding images of all reference points, then the minimum value of all intensity offsets is the most similar scene. When the is less than c_m, it means that the same view is matched and the head-direction angle of the image being compared is the same as the real angle. When the image of the starting position is re-detected, the robot rotates exactly once. The angles of all the cognitive points were updated with the equation (γ_n represents the position of neural activity on the circular model as the robot rotates once back to its starting position). All cognitive nodes are defined as reference points.

Step3: Update of reference points. The optical flow algorithm is greatly affected by environmental factors, so there is an error between the reference point constructed by the robot with only one rotation and the real head-direction angle of the point, which cannot be used as the reference point for the HDCs development. Therefore, it is necessary to rotate the robot several times on the basis of Step1, detect the reference point by using step2, and record the angle data set of the corresponding reference point in the multiple rotation of the robot. Then, the angle at the *i*-th reference point is as follows:

$$\overline{\theta}_i=\frac{\sum_{j=1}^{K}\theta_{ij}-max\left(\theta_{ij}\right)-min\left(\theta_{ij}\right)}{K-2} \tag{14}$$

In Eq. (14), represents the total number of rotation cycles of the robot, represents the angle value at the *i*-th closed-loop point when the robot rotates circles. The purpose of subtracting the maximum and minimum values is to eliminate the influence of accidental factors in the experiment, so that the angle at the reference point is closer to the real head-direction angle.

Step4: Development of the mode. Then rotate the robot arbitrarily and use the strength of scanning line to detect whether the closed-loop point is reached, using a PI controller to adjust the sensory gain β, the mathematical expression is as follows:

$$\beta=k_p(\gamma_i-\gamma_t)+k_i\int_{t=0}^{T}(\gamma_i-\gamma_t)dt \tag{15}$$

In Eq. (15), and respectively represent the proportion and integral coefficient of the regulator, represents the head-direction angle corresponding to the closed-loop point, represents the head direction angle at the current moment. After adjusting the gain and resetting the annular cell model, so that the location of the activity package on the annular model was at the same angle as the real head direction. Thus, by multiple resets of neural activity and the adjustment of the factor, the rate at which the activity packets move on the annular model will gradually be consistent with the rate at which the real head-direction angle changes.

Step5: Developmental maturity determination. The development maturity of HDCs is defined as $\vartheta=\frac{\gamma_i-\gamma_{i-1}}{\theta_i-\theta_{i-1}}$, including and represent the current detected point moment and last closed-loop moment of the activity package location and real head-direction angle. The closer the value of is to 1, the closer location of the activity package and the real head-direction angle, the cells develop more mature.

4 EXPERIMENTS AND FINDINGS

4.1 Robot $

Main platform adopted in the experiment is a mobile robot with four-wheel independent drive and differential steering. The robot platform is shown in Figure 3. Kinect RGB-D camera is placed above the platform panel and is powered by an inverter. A gyroscope sensor is built into the body to obtain current direction information. The robot communicates with the computer through WIFI and controls the rotation angular velocity and direction of the robot. Meanwhile, the robot can feed back the information of various sensors to the computer for calculation. In order to check the accuracy of the experiment, an electronic compass was installed on the robot platform as the absolute reference of real head-direction angle.

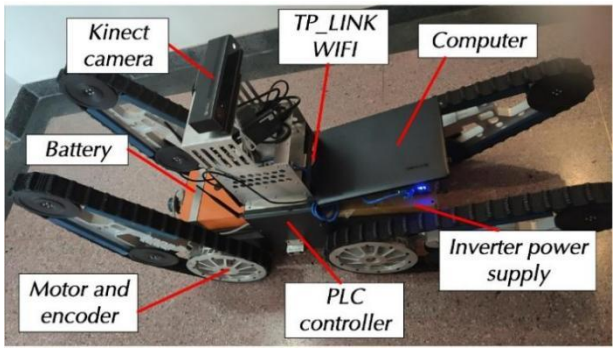

Figure 3 Schematic Diagram of Robot Platform

4.2 HDCs Development Experiment

The robot platform is used to collect data sets in the laboratory environment. The image size for visual matching is unified into 500 * 1000. The rotation direction of the robot is counterclockwise, and the angular velocity is set as $\left(0\sim\frac{pi}{5}\right)rad/s$. The sampling period is set as 0.2s. The value of the angle integral constant is set as 0.5. The number of cells in the annular model is set as 36. The distribution width constant of neural activity is set as 4. The control overall level is set as 0.00002. The comparison threshold is set as 0.23. The optical flow vector and the annular model between the continuous images generated by robot rotation during the experiment is shown in Figure 4.

From Figure 4, it can be seen that as the robot rotates, it can generate strong horizontal optical flow vectors, driving the movement of the activity packet on the annular cell model. Subsequently, conduct developmental experiments of HDCs in three different indoor environments. Let the robot rotate multiple times, and to ensure the stability of the subsequent development process, select the top 100 images with the highest similarity in closed-loop detection under each task as the set of angle reference points, as shown in Figure 5. The statistics of angle errors for all reference points under different numbers of rotation cycles are shown in Figure 6(a), the statistics of the average angle errors of reference points under

different numbers of rotation cycles is shown in Figure 6(b).

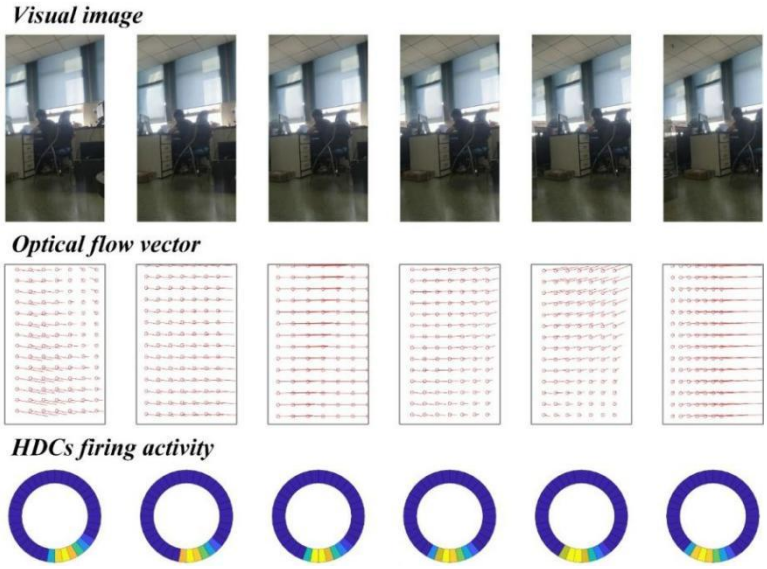

Figure 4 Effect of Optical Flow Driven Activity Package Moving on the Circular Model

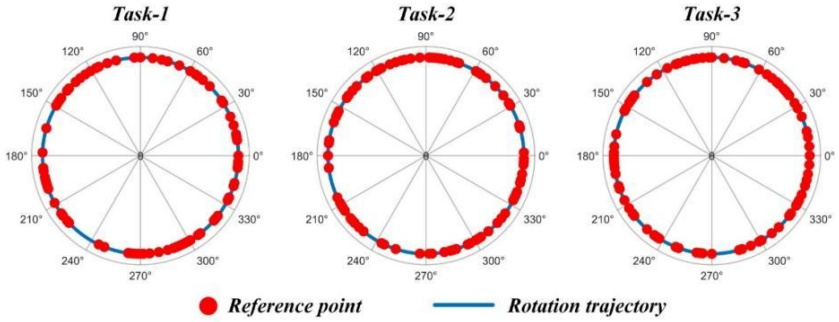

Figure 5 The Establishment of the Set of Angle Reference Points

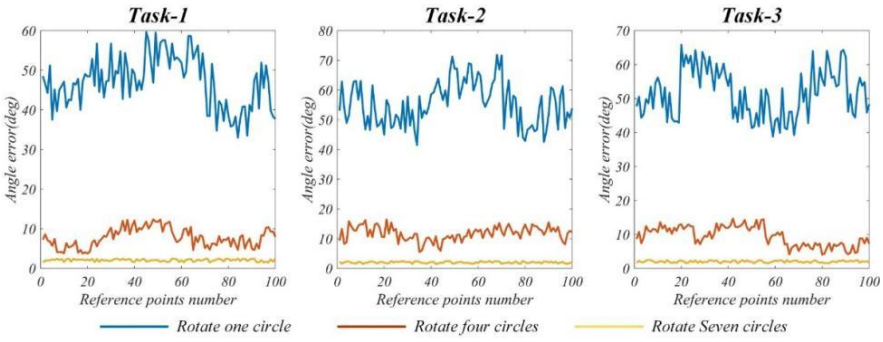

(a) Angle errors for all reference points under different numbers of rotation cycles

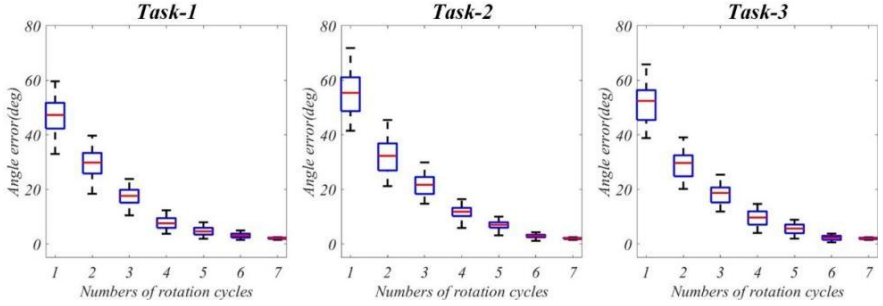

(b) Average angle errors of reference points under different numbers of rotation cycles

Figure 6 Angle Errors of the Reference Points Varies with the Number of Rotations

From Figure 6, it can be observed that as the number of rotation cycles increases, the angle errors of all reference points

gradually decrease. The core reason is that multiple rotations, through averaging with the removal of extreme values, reduce optical flow noise and random errors, making the reference point angles closer to the true values. After obtaining the precise angles of the reference points, the developmental experiment for HDCs can be conducted. The rotational angular velocity of the robot is randomly selected within the range of $\left(-\frac{pi}{10} \sim \frac{pi}{7}\right) rad/s$, and the frequency of change in rotational angular velocity is 2Hz. The parameters of the PI controller affect the developmental process of HDCs. Therefore, through multiple experiments, selecting and allows the model to converge quickly. During the developmental process, the changes in the calculated and actual values of the head direction angle are shown in Figure 7(a), and the changes in the developmental maturity of HDCs are shown in Figure 7(b).

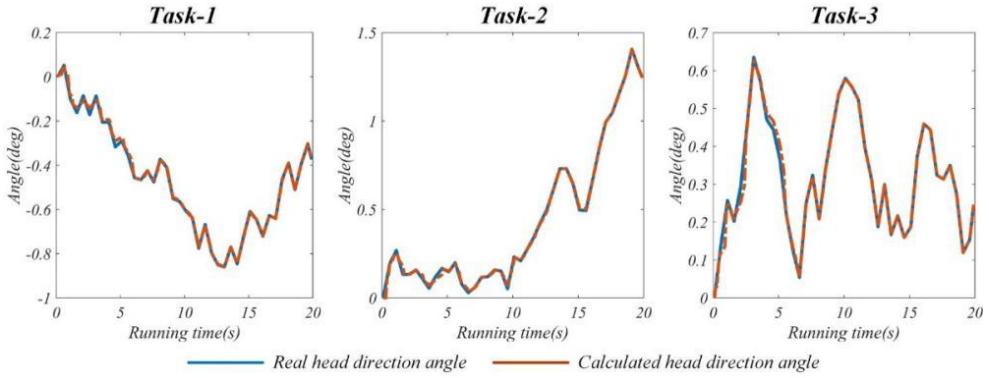

(a) The changes in the calculated and actual values of the head direction angle

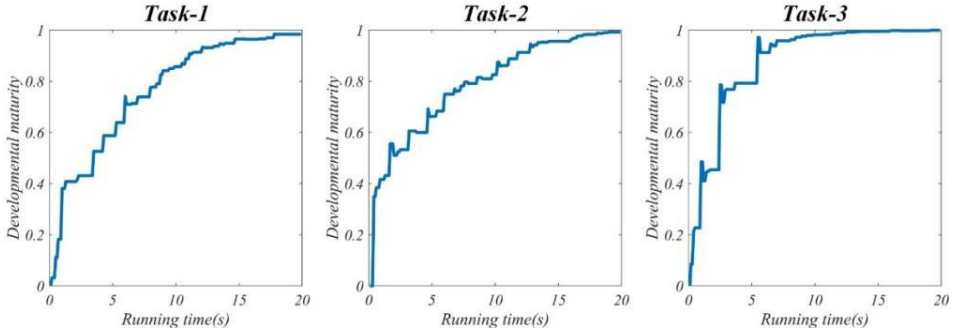

(b) The changes in the developmental maturity of HDCs

Figure 7 Experimental Results of HDCs Development

Figure 7(a) shows that the model's calculated head direction angle initially deviates significantly from the actual angle due to optical flow noise and unoptimized vestibular gain, leading to error accumulation. However, through closed-loop correction using visual template matching and PI controller, the calculated angle gradually synchronizes with the actual angle after multiple rotations, with the error significantly reduced and ultimately approaching zero. Figure 7(b) indicates that the maturity of HDCs starts at a low value, rises progressively with fluctuations tied to closed-loop detection, and eventually approaches 1, reflecting the transition from immaturity to maturity. This is driven by precise updates of the reference point set and dynamic gain adjustments during multiple rotations, effectively simulating the visually dominated HDCs development process in the rat brain and validating the model's bio-inspired potential for accurate navigation with low hardware dependency.

4.3 Comparative Experiment

The accumulative error is a difficult problem in the robot navigation system, which is usually caused by the inaccuracy and drift of the sensor information. To verify the accuracy of the model, the following experiments are designed: the angle of the electronic compass is taken as the reference quantity of the experiment (the real head-direction angle), and the output angle of the model is compared with the angle of the gyroscope and the angle of the gyroscope after EKF filter [31]. In the physical environment of the second group of experiments, the robot was rotated in the counterclockwise direction and the clockwise direction respectively from the starting point. The rotational angular velocity is randomly selected within the range of $\left(\frac{pi}{23} \sim \frac{pi}{18}\right) rad/s$, and the frequency of change in angular velocity is 1Hz. The experimental results are shown in Figure 8.

From Figure 8, it can be observed that the raw gyroscope angle exhibits a significant accumulation of error as time progresses. This is due to the inherent drift and noise in the gyroscope, which amplify errors during long-term integration, leading to substantial deviations. In contrast, the gyroscope angle filtered by EKF shows a slower increase in error, with a smaller overall deviation. This indicates that EKF partially suppresses random errors and biases in the gyroscope through state estimation and noise modeling, improving accuracy, but it cannot fully eliminate systematic drift, especially in

environments with frequent dynamic angular velocity changes. The proposed model demonstrates the flattest error curve, remaining close to zero or fluctuating within a small range, and even stabilizing after multiple rotations, significantly outperforming traditional sensor methods.

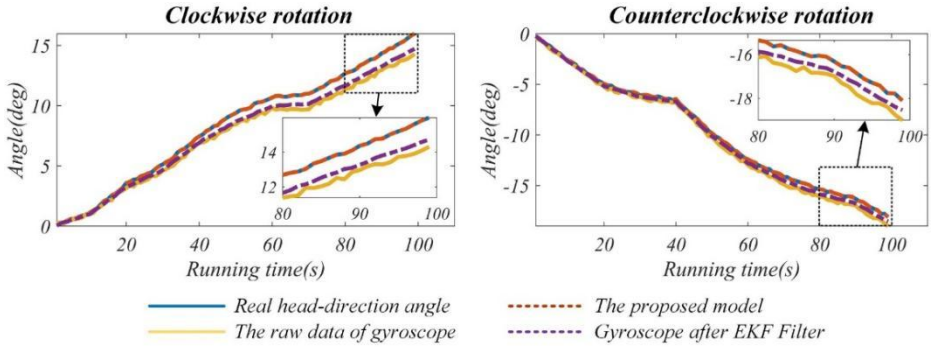

Figure 8 Comparison Diagram of Cumulative Error Experimental Results

5 CONCLUSION

This study presents a novel biologically inspired computational model for the development of head-direction cells (HDCs) in the rat brain, leveraging visual input as the primary sensory cue. By constructing a one-dimensional annular cell model driven by optical flow and incorporating a closed-loop correction mechanism with visual template matching and a PI controller, the model successfully simulates the maturation process of HDCs. Experimental results demonstrate that the model achieves precise synchronization between the neural activity package and the actual head-direction angle, with cumulative errors significantly reduced compared to traditional sensor-based methods like gyroscopes and EKF-filtered gyroscopes. The model's ability to dynamically adjust vestibular gain and reset firing activity ensures robust and accurate head-direction estimation, even in dynamic environments, with minimal hardware requirements.

The proposed model not only advances our understanding of HDCs development by replicating the visually dominated maturation process observed in biological systems but also offers practical implications for bio-inspired robotic navigation. By addressing the limitations of traditional sensors, such as error accumulation, the model provides a low-cost, efficient alternative for achieving reliable spatial orientation. Future work could extend this model by integrating additional sensory modalities, such as proprioceptive or auditory cues, to further enhance its robustness and applicability in complex, real-world environments. Additionally, exploring the model's scalability to larger neural networks or its adaptation to other species could deepen insights into the neural basis of spatial cognition and its application to autonomous systems.

COMPETING INTERESTS

The authors have no relevant financial or non-financial interests to disclose.

FUNDING

This work was supported in part by the Early-Career Young Scientists and Technologists Project of Jiangxi Province under Grant 20252BEJ730116, in part by the Science and Technology Research Project of Jiangxi Provincial Department of Education under Grant GJJ2400402.

REFERENCE

[1] Basu J, Nagel K. Neural circuits for goal-directed navigation across species. Trends Neuroscience, 2024, 47: 904-917.
[2] Fenton AA. Remapping revisited: how the hippocampus represents different spaces. Nature Reviews Neuroscience, 2024, 25: 428-448.
[3] Ouchi A, Fujisawa S. Predictive grid coding in the medial entorhinal cortex. Science, 2024, 385: 776-784.
[4] Blanco-Hernández E, Balsamo G, Preston-Ferrer P, et al. Sensory and behavioral modulation of thalamic head-direction cells. Nature Neuroscience, 2024, 27: 28-33.
[5] Campbell MG, Giocomo LM. Self-motion processing in visual and entorhinal cortices: inputs, integration, and implications for position coding. Journal of Neurophysiology, 2018, 120: 2091-2106.
[6] Moser EI, Moser MB, McNaughton BL. Spatial representation in the hippocampal formation: a history. Nature Neuroscience, 2017, 20: 1448-1464.
[7] Wills TJ, Cacucci F, Burgess N, et al. Development of the hippocampal cognitive map in preweanling rats. Science, 2010, 328: 1573-1576.
[8] Taube JS, Muller RU, Ranck JB. Head-direction cells recorded from the postsubiculum in freely moving rats. I. Description and quantitative analysis. Journal of Neuroscience, 1990, 10: 420-435.

[9] Taube JS. The head direction signal: origins and sensory-motor integration. Annual Review of Neuroscience, 2007, 30: 181-209.
[10] Chen G, Manson D, Cacucci F, et al. Absence of visual input results in the disruption of grid cell firing in the mouse. Current Biology, 2016, 26: 2335-2342.
[11] Graham JA, Dumont JR, Winter SS, et al. Angular head velocity cells within brainstem nuclei projecting to the head direction circuit. Journal of Neuroscience, 2023, 43: 8403-8424.
[12] Keshavarzi S, Velez-Fort M, Margrie TW. Cortical integration of vestibular and visual cues for navigation, visual processing, and perception. Annual Review of Neuroscience, 2023, 46: 301-320.
[13] Staiger JF, Petersen CCH. Neuronal circuits in barrel cortex for whisker sensory perception. Physiological Reviews, 2021, 101: 353-415.
[14] Keshavarzi S, Bracey EF, Faville RA, et al. Multisensory coding of angular head velocity in the retrosplenial cortex. Neuron, 2022, 110: 532-543.
[15] Madhav MS, Jayakumar RP, Li BY, et al. Control and recalibration of path integration in place cells using optic flow. Nature Neuroscience, 2024, 27: 1599-1608.
[16] Zeil J. Visual navigation: properties, acquisition and use of views. Journal of Comparative Physiology A, 2023, 209: 499-514.
[17] Fortenberry B, Gorchetchnikov A, Grossberg S. Learned integration of visual, vestibular, and motor cues in multiple brain regions computes head direction during visually guided navigation. Hippocampus, 2012, 22: 2219-2237.
[18] Bing Z, Sewisy AEI, Zhuang G, et al. Toward cognitive navigation: Design and implementation of a biologically inspired head direction cell network. IEEE Transactions on Neural Networks and Learning Systems, 2021, 33: 2147-2158.
[19] Evans T, Bicanski A, Bush D, et al. How environment and self-motion combine in neural representations of space. Journal of Physiology, 2016, 594: 6535-6546.
[20] Cullen KE. The vestibular system: multimodal integration and encoding of self-motion for motor control. Trends in Neurosciences, 2012, 35: 185-196.
[21] Stein BE, Stanford TR, Rowland BA. Multisensory integration and the Society for Neuroscience: then and now. Journal of Neuroscience, 2020, 40: 3-11.
[22] Milford MJ, Wyeth GF. Mapping a suburb with a single camera using a biologically inspired SLAM system. IEEE Transactions on Robotics, 2008, 24: 1038-1053.
[23] Zou Q, Cong M, Liu D, et al. A neurobiologically inspired mapping and navigating framework for mobile robots. Neurocomputing, 2021, 460: 181-194.
[24] Zhang Z, Tang F, Li Y, et al. A spatial transformation-based CAN model for information integration within grid cell modules. Cognitive Neurodynamics, 2024, 18: 1861-1876.
[25] Massoud TM, Horiuchi TK. A neuromorphic VLSI head direction cell system. IEEE Transactions on Circuits and Systems I: Regular Papers, 2010, 58: 150-163.
[26] Page HJI, Walters D, Stringer SM. Architectural constraints are a major factor reducing path integration accuracy in the rat head direction cell system. Frontiers in Computational Neuroscience, 2015, 9: 10.
[27] Vafidis P, Owald D, D'Albis T, et al. Learning accurate path integration in ring attractor models of the head direction system. eLife, 2022, 11: e69841.
[28] Westeinde EA, Kellogg E, Dawson PM, et al. Transforming a head direction signal into a goal-oriented steering command. Nature, 2024, 626: 819-826.
[29] Sun Z, Ma K, Xia S, et al. BIG: a framework integrating brain-inspired geometry cell for long-range exploration and navigation. Satellite Navigation, 2025, 6: 1-20.
[30] Baker S, Matthews I. Lucas-Kanade 20 years on: A unifying framework. International Journal of Computer Vision, 2004, 56: 221-255.
[31] Ribeiro MI. Kalman and extended kalman filters: Concept, derivation and properties. Institute for Systems and Robotics, 2004, 43: 3736-3741.